Sequential Activation of Molecular Breathing and Bending during Spin-Crossover Photoswitching Revealed by Femtosecond Optical and X-Ray Absorption Spectroscopy

Marco Cammarata,[1] Roman Bertoni,[1] Maciej Lorenc,[1] Hervé Cailleau,[1] Sergio Di Matteo,[1] Cindy Mauriac,[2]
Samir F. Matar,[2] Henrik Lemke,[3] Matthieu Chollet,[3] Sylvain Ravy,[4] Claire Laulhé,[4]
Jean-François Létard,[2] and Eric Collet[1,*]

[1]*Institut de Physique de Rennes, UMR CNRS 6251, Université Rennes 1, 35042 Rennes Cedex, France*
[2]*CNRS, Université de Bordeaux, ICMCB, 87 Avenue du Dr. A. Schweitzer, Pessac 33608, France*
[3]*LCLS, SLAC National Laboratory, Menlo Park, California 94025, USA*
[4]*Synchrotron SOLEIL, L'Orme des Merisiers, Saint Aubin, 91192 Gif-sur-Yvette, France*

We study the basic mechanisms allowing light to photoswitch at the molecular scale a spin-crossover material from a low- to a high-spin state. Combined femtosecond x-ray absorption performed at LCLS X-FEL and optical spectroscopy reveal that the structural stabilization of the photoinduced high-spin state results from a two step structural trapping. Molecular breathing vibrations are first activated and rapidly damped as part of the energy is sequentially transferred to molecular bending vibrations. During the photoswitching, the system follows a curved trajectory on the potential energy surface.

Introduction.—A wide range of phenomena in matter are driven by changes that occur after illumination with light [1]. This includes chemical, biochemical, or solid-state reactions [2–4], as well as switching of functionality of materials such as conductivity [5] or magnetism [6]. During a transformation triggered by a femtosecond (fs) laser pulse the excited system is launched onto a complex pathway, from the initial photoexcited to the final photoinduced state, whereby nonequilibrium phenomena, coherent dynamics, and interconversion of energy are interconnected [1]. Transition metal complexes undergoing spin crossover (SCO) from low-spin (LS) to high-spin (HS) state are prototypes of molecular photoswitching in materials [7]. On the shortest time scales the molecule undergoes intersystem crossing (ISC) from the initial photoexcited LS to HS state. The structural reorganization of the ligand around the metal center gives rise to an energy barrier between the trapped HS and the ground LS state. The initial mechanism behind the extremely fast ISC, between states that differ in both spin and structure, defies conventional descriptions. Recent theoretical studies by van Veenendaal [8,9] on ISC in Fe[II] SCO, mediated by the spin-orbit coupling, discussed the role of significant changes of the metal-ligand distance (molecular breathing). It was proposed that the ultrafast ISC results from the dephasing of the photoexcited state into the HS phonon states. A monotonic decay of the photoexcited state to the HS state becomes efficient when this breathing mode is rapidly damped as energy is dissipated into the environment.

By combining femtosecond x-ray absorption near edge structure (XANES) and optical spectroscopy, we provide an experimental evidence of the ultrafast activation and damping of molecular breathing accompanying the ISC,

which was lacking up to now. This process is followed by vibrational cooling in the HS potential observed on the bending mode. With respect to conventional models describing SCO photoswitching in terms of the potential energy curve along a single breathing coordinate, our work reveals a more complex reality involving a curved trajectory, along breathing and bending, on a multidimensional potential energy surface.

Results.—The SCO $[Fe(phen)_2(NCS)_2]$ crystal investigated here undergoes a first-order phase transition from LS ($S = 0$, $t_{2g}^6 e_g^0 L^0$) to HS ($S = 2$, $t_{2g}^4 e_g^2 L^0$) states above ≈ 180 K and exhibits photomagnetism and photochromism [7,10,11]. Here, L corresponds to the LUMO of the ligand. This molecular bistability is associated with important structural reorganizations around the FeN_6 octahedron between both spin states [see Fig. 1(a), Fig. S1 and Fig. S2 in the Supplemental Material [12], and Refs. [13–18]]. The less bonding character of the HS state leads to the expansion of the average Fe-N bond length from $\langle Fe - N \rangle_{LS} = 1.97$ to $\langle Fe - N \rangle_{HS} = 2.16$ Å, often observed for Fe[II] SCO [7,19]. That changes the XANES spectrum as shown in Fig. 1(b), in agreement with the published data on this molecular crystal [20].

The ultrafast photoswitching dynamics of $[Fe(phen)_2(NCS)_2]$ is investigated in the LS phase at 140 K by two complementary pump-probe methods [12]. A ≈ 50 fs laser pulse (650 nm) photoswitches the LS state to HS via a metal-to-ligand charge-transfer process (MLCT) [10]. The changes in XANES are recorded with ≈ 30 fs x-ray pulses at the XPP station of the LCLS X-FEL [21], while changes in optical reflectivity (OR) and transmission (OT) are recorded with ≈ 50 fs visible-near infrared spectroscopy. Figure 2(a) shows the time course of the XANES signal
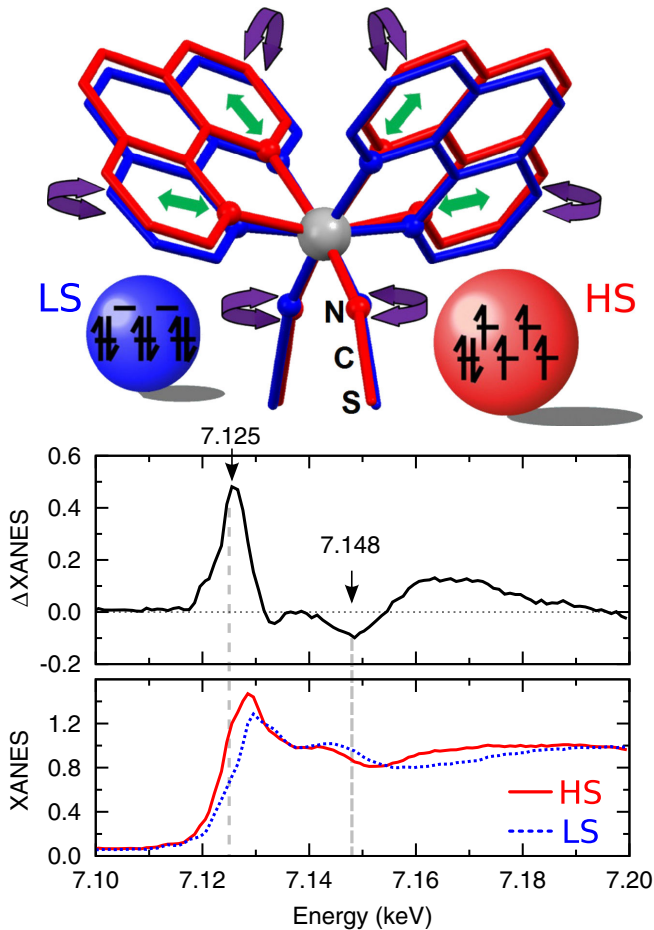
FIG. 1 (color online).   (a) LS (140 K, blue) and HS (200 K, red) structures of $[Fe(phen)_2(NCS)_2]$ (phen = 1, 10-phenanthroline). The central Fe atom is bounded by N to the phenantroline and NCS groups. Green arrows represent the breathing mode and purple ones the bending mode. (b) XANES spectra and difference ΔXANES measured between the LS and HS states.

FIG. 2 (color online).   Kinetic traces of XANES at 7125 and 7148 eV, fit with a single-exponential function of the rising edge [$\tau_{Fe-N} = 170$ (10) fs] represented by red solid lines (a). Kinetic traces of OR and OT at 760 nm (b), OR at 900 and 550 nm and OT at 900 nm (c) and OT 850 nm (d). Fits by a single-exponential function describing the fast change plus a fifth order polynomial are represented by red solid lines.

measured at two energies most sensitive to the structural change (Fig. 1). The increase of the XANES signal at 7.125 keV and the decrease at 7.148 keV mainly result from Fe-N elongation [20] and are the fingerprints of the formation of HS structures. We fit the rising time by convolving a GAUSSIAN temporal instrument response function (IRF) with an exponential rise (τ_{Fe-N}). The 110 (10) fs FWHM IRF, obtained by using a timing tool [21] designed to synchronize the optical and the x-ray laser pulses, allows an accurate determination of $\tau_{Fe-N} = 170$ (20) fs.

Figures 2(b)–2(d) and S4 in the Supplemental Material [12] show time traces of OR and OT (with 110 fs IRF) in different spectral zones, revealing two main steps: the onset of OR change or a peak in OT immediately after laser excitation, relaxing towards a plateau during the first hundreds of femtoseconds. The increase of optical absorption on the plateau, which translates into a simultaneous decrease of OR and OT in all probed regions, is another fingerprint of the LS-to-HS photoswitching, also
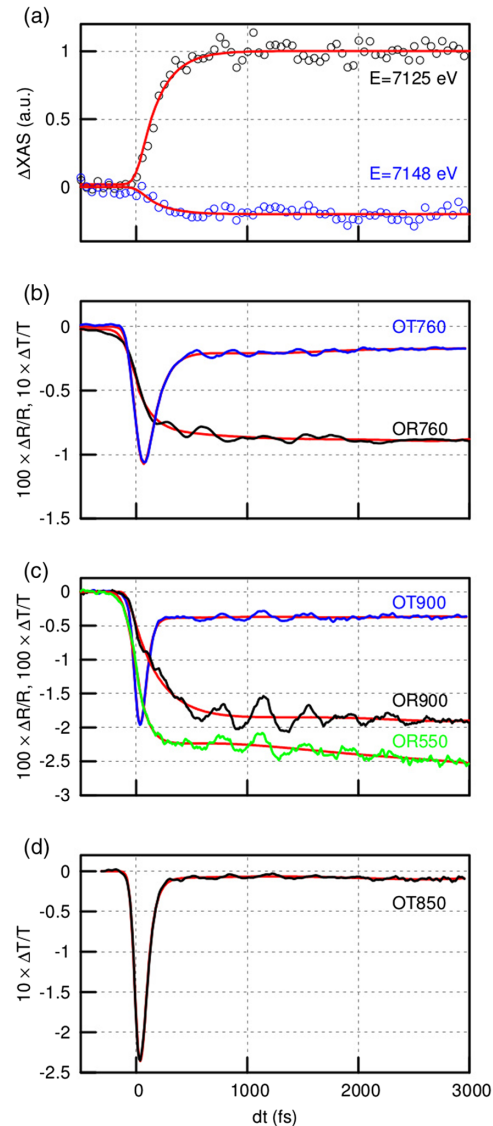
observed during the thermal LS-to-HS conversion [10] (see also Fig. S3 in [12]). Density of state calculations [16] explain the stronger absorption of the HS state around 760 nm (1.6 eV) by a decrease of the energy gap between the t_{2g} and e_g bands from ≈1.9 (LS) to ≈1.6 eV (HS), due to the molecular ligand field weakening (see also Fig. S5 in [12]). OT and OR data at 760 nm indicate that the gap narrowing in the HS state, resulting from the Fe-N elongation, occurs within $\tau_{Fe-N} = 140$ (20) fs. It correlates well with the 170 (20) fs time constant obtained by XANES.

The transient OT peak corresponds to the absorption of the photoexcited singlet ^{1}MLCT state ($t_{2g}^5 e_g^0 L^1$), and other

possible intermediate (INT) electronic states [9], and results from transition from a ligand level L to higher energy states (see Fig. S5) [10,12]. 760 nm therefore probes both INT and HS ($t_{2g} - e_g$) absorptions. The $t_{2g} - e_g$ absorption is no more accessible at 850 nm and above, and the main effect in the time traces is the absorption of the INT electronic state. This transient OT peak above 850 nm [Figs. 2(c) 2(d) and S4 in the Supplemental Material [12]] better characterizes the depopulation of the INT state, which decays within less than 50 fs. Thus far, our results determine an ISC of tens of fs and a ≈ 160 fs Fe-N bond elongation in a solid, both of which are similar to those reported for Fe^{II} molecules in solution [22–27].

On top of such changes, clear oscillating components are present in the optical data. Figures 3(a)–3(c) show the residuals after exponential fit. Data at 760 nm show a coherent vibration around 113 cm^{-1} (≈ 300 fs oscillation period) in the [0–700 fs] range. The corresponding time-dependent Fourier transforms are presented in Figs. 3(d)–3(f) and S4 in [12], and the apparent rising time of the 113 cm^{-1} mode is limited by the GAUSSIAN temporal window used [12]. It was already discussed above that OT and OR at 760 nm are sensitive to the Fe-N elongation, hereafter referred to as the breathing coordinate D. Therefore, the oscillations riding on 760 nm signals reflect the breathing mode, i.e., the totally symmetric Fe-N stretching, in relation with the symmetry conserving picture of the displacive spin-state switching. This observation is supported by calculations, according to which the only totally symmetric mode (symmetry A in the C_2 point group of the complex) in this frequency range is the breathing mode (≈ 125 cm^{-1}) in the HS state [28,29]. The breathing mode is represented by green arrows in Fig. 1 and shown in the Supplemental Material, video S1 [12]. XANES data do not reveal such small oscillating features after the ≈ 0.2 Å elongation, because of the noise limit of the measurements, but we underline that the main Fe-N elongation occurs on a time scale approaching the half period of the breathing mode [Fig. 4(a)].

Optical data at 550, 900 nm [Fig. 2(c)] and 950 nm (Fig. S4 in the Supplemental Material [12]) reveal another coherent vibration, in-phase for all these probing wavelengths. These oscillations around 85 cm^{-1} correspond to the butterfly mode (also of A symmetry) [28,29], which bends the ligand and the N-Fe-N angles without significantly changing Fe-N distances (see purple arrows in Fig. 1 and video S2 in the Supplemental Material [12]). This is a bending coordinate Σ [19,30] and such a coherent ligand vibration was also observed for another Fe^{II} SCO molecular system in solution [25]. Unlike the breathing mode, we observed that the bending mode with ≈ 390 fs period is only activated coherently during a second step, after ≈ 500 fs, with a maximum spectral weight around 1300 fs (Figs. 3, and S4 in [12]).
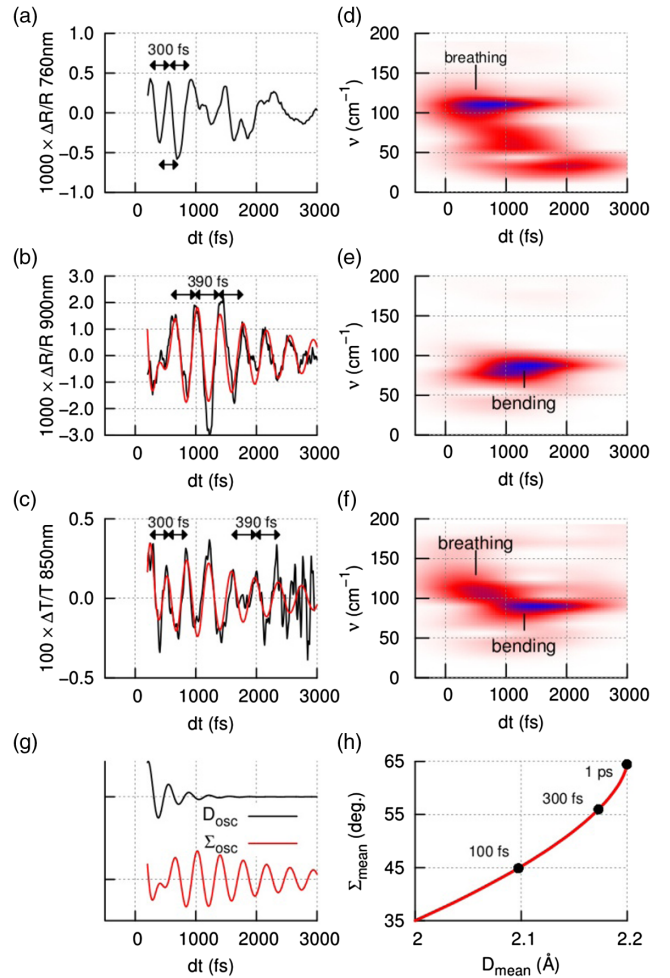

FIG. 3 (color online).   (a)–(c) Oscillating component of OR at 760, OR at 900, and OT at 850 nm. (d)–(f) Time dependent FFT of the experimental data, showing the activation of the breathing mode and the delayed activation of the bending mode. Combined fits of OR at 900 nm and OT at 850 nm (red line) by the coupled oscillator model, which show the contribution of the bending (Σ) mode (b) and the superposition of bending (Σ) and breathing (D) modes. (c) The time course of the oscillating component D_{osc} (300 fs) and Σ_{osc} (390 fs) obtained by the fit in (b) and (c) are displayed in (g) and the average evolutions of D_{mean} and Σ_{mean} obtained by the fit in Fig. 3 are displayed in (h).

This bending occurs well after the 160 fs initial Fe-N elongation.

Such oscillations cannot be attributed to impulsive Raman process in the ground LS state because the LS breathing frequency is significantly higher (156 cm^{-1}) [28,29]. In addition, there are no optical transitions from the LS state to other excited states which can be probed in the 760–950 nm region (Fig. S5 [12]) and, consequently, the LS state is optically silent in our data.

Discussion.—In SCO materials the Fe-N elongations during LS-to-HS conversion are very similar, but the ligand bending Σ [12,19,30] also plays an important role for the relative stability of LS and HS states. Hauser evidenced in
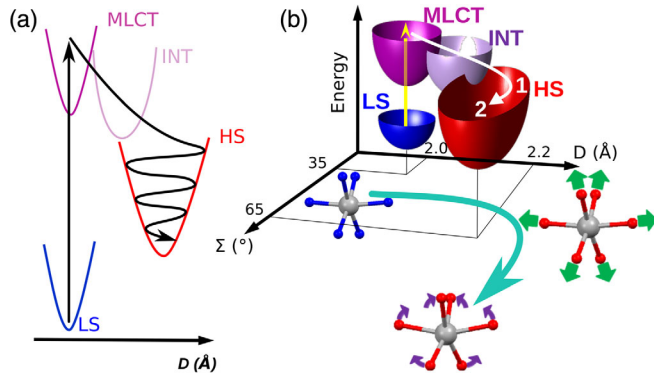
FIG. 4 (color online). (a) Schematic representation of the elongation and damping of the breathing mode along the D coordinate. (b) Classical trajectory in the (D, Σ) space. Molecules in the LS (blue) potential reach the ^{1}MLCT state by light excitation. Fast ISC, through possible INT states, drives D elongation during step 1 with the generation and damping of breathing phonon, followed by activation of additional bending phonons such as distortion Σ, during step 2. The sequence is sketched at the bottom.

the kinetic studies of HS → LS relaxation a breakdown of the single mode model and proposed to describe such systems by qualitatively splitting the reaction coordinate into the breathing and the bending modes [31]. Figure 4(b) is a cartoon of a likely potential energy surface (PES) of $[\text{Fe(phen)}_2(\text{NCS})_2]$ in the breathing and bending (D, Σ) coordinate space. At thermal equilibrium (see Ref. [13] and Fig. S2 in the Supplemental Material [12]) the LS potential is centered at $(D_{\text{LS}} = 1.97$ Å, $\Sigma_{\text{LS}} = 35°)$ and the one of the HS state at $(D_{\text{HS}} = 2.16$ Å, $\Sigma_{\text{HS}} = 65°)$. The delayed activation of the bending Σ, with respect to breathing D is schematically represented in Fig. 4(b) on (D, Σ) PES from stable LS to stable HS locations.

XANES, OT, and OR data at 760 nm give an average elongation $D_{\text{mean}}(t)$ with a ≈160 fs time constant. OR at 900 nm, no more sensitive to D but only to the change of Σ, gives an average torsion $\Sigma_{\text{mean}}(t)$ with 250 fs time constant. We thus deduce from these different breathing and bending time scales a curved trajectory in the relevant coordinate space (D, Σ) on PES. If we simply assume that the photoinduced HS state is not significantly different from the HS structure at thermal equilibrium, we can plot a trajectory in Fig. 3(h). It indicates that around 1 ps the motion is mainly along Σ, also simultaneously manifested by the strong spectral weight of the bending mode [Figs. 3(e)–3(f)]. The coupling of instantly photoactivated phonons to other modes can drive major structural reorganization in solids [4,32,33]. In the present case, the energy transfer between the two totally symmetric breathing (D) to bending (Σ) modes can be described by a linear coupling, with the classical equations of motion of coupled harmonic oscillators,

$$\mu_D \ddot{D} + \gamma_D \dot{D} + k_D D + k_{D\Sigma}(D - \Sigma) = 0$$
$$\mu_\Sigma \ddot{\Sigma} + \gamma_\Sigma \dot{\Sigma} + k_\Sigma \Sigma - k_{D\Sigma}(D - \Sigma) = 0.$$

μ_i are the reduced masses of the oscillators (obtained from GAUSSIAN calculations [12]), k_i are the force constants refined to reproduce 113 and 85 cm^{-1} frequencies of the oscillations, γ_i/μ_i are the damping rates and $k_{D\Sigma}$ is the coupling between the two modes. A numerical fit of the oscillating part of the time dependent data [12] with these equations of motion gives the time evolution of the oscillating components $D_{\text{osc}}(t)$ and $\Sigma_{\text{osc}}(t)$ [Fig. 3(g)]. These curves reproduce well the initial activation of the 113 cm^{-1} breathing oscillation, in agreement with the displacive description of the ISC along D. The fit also evidences a very fast damping of the breathing mode within 166 fs ($\gamma_D/\mu_D = 6$ ps^{-1}). These results are in agreement with the theoretical model [8] introduced above, which considers an ISC of tens of femtoseconds accompanied by a structural elongation of the order of 100–200 fs and a damping time constant shorter than the period of the breathing mode (300 fs here). The observed delayed coherent activation of Σ characterizes the energy transfer from the breathing to the bending modes schematically represented in Fig. 4(b) and the smaller damping of the bending mode ($\gamma_\Sigma/\mu_\Sigma = 1.16$ ps^{-1}) indicates that the system oscillates (in the HS potential) as it gets vibrationally cooled within 900 fs. The additional transfer to other modes, for instance to lower frequency optical lattice phonons, can also be considered. A lattice mode is observed at 33 cm^{-1} [Fig. 3(d)], but its spectral weight is weaker. Thus, the major part of energy of the absorbed photon (1.9 eV) is dissipated, since each coherent molecular phonon only accounts for a small fraction of that energy. For instance, the energy of the breathing mode, $E = (1/2)\,m\omega^2 D^2$, can be estimated to only 40 meV, with reduced mass $m = 8.5$ amu, angular frequency $\omega = 2\pi \times 113$ cm^{-1}, and elongation $D \approx 0.2$ Å.

Conclusion.—In the emerging field of control science, understanding the physical processes allowing functionalization with light on an ultrafast time scale is a key issue. Our results confirm the fast intersystem crossing observed in such transition-metal systems [22–27], as the change of electronic state is shorter than 50 fs and followed by a significant metal-ligand elongation within 160 fs. This initial structural change is directly coupled to the change of electronic state because of the less bonging nature of the HS state. Our experimental studies more importantly provide an experimental demonstration that the fast and highly efficient ISC is driven by the dephasing of the photoexcited state into the HS phonon states. The activated breathing mode is damped on a time scale (160 fs) close to its half period, which allows an efficient trapping in the HS state as the decrease of the oscillation amplitude hinders recurrence to the initial state. We also show that the molecular bending is involved too, since the Fe-N elongation once established

triggers the increase of the N-Fe-N bending because of ligand rigidity. Its delayed activation reveals a curved trajectory on a multidimensional potential energy surface, which underlines the limits of conventional descriptions along a single breathing coordinate on potential energy curves. This description of the photoswitching at the molecular scale, accompanied by important energy redistribution, sets the initial conditions for the slower transformation at the material scale [34,35]. Such combinations of x-ray and optical spectroscopies are key to disentangling the role of different degrees of freedom of electronic and/or structural nature in photoinduced phenomena.

*To whom correspondence should be addressed.
  eric.collet@univ-rennes1.fr

[1] *Photoinduced Phase Transitions*, edited by K. Nasu (World Scientific, Singapore, 2004).

[2] V. S. Petrovic *et al.*, Phys. Rev. Lett. **108,** 253006 (2012).

[3] D. Polli *et al.*, Nature (London) **467,** 440 (2010).

[4] H. Uemura and H. Okamoto, Phys. Rev. Lett. **105,** 258302 (2010).

[5] M. Gao *et al.*, Nature (London) **496,** 343 (2013).

[6] A. Kirilyuk, A. V. Kimel, and T. Rasing, Rev. Mod. Phys. **82,** 2731 (2010).

[7] *Spin-Crossover Materials*, edited by M. Halcrow (Wiley, West Sussex, 2013).

[8] M. van Veenendaal, J. Chang, and A. J. Fedro, Phys. Rev. Lett. **104,** 067401 (2010).

[9] J. Chang, A. J. Fedro, and M. van Veenendaal, Phys. Rev. B **82,** 075124 (2010).

[10] E. König and K. Madeja, Inorg. Chem. **6,** 48 (1967).

[11] E. W. Müller, H. Spiering, and P. Gütlich, Chem. Phys. Lett. **93,** 567 (1982).

[12] See Supplemental Material at http://link.aps.org/supplemental/10.1103/PhysRevLett.113.227402, which includes Refs. [13–18], for information on the x-ray

[13] J. A. Real, B. Gallois, T. Granier, F. Suez-Panama, and J. Zarembovitch, Inorg. Chem. **31,** 4972 (1992).

[14] P. Ganguli, P. Gütlich, and P. Müller, Inorg. Chem. **21,** 3429 (1982).

[15] M. J. Frisch *et al.*, GAUSSIAN03, revision C.02 (Gaussian, Inc., Wallingford, CT, 2004).

[16] S. Matar and J. F. Létard, Z. Naturforsch. **65B,** 565 (2010).

[17] E. Jones *et al.*, SciPy: Open Source Scientific Tools for Python, http://www.scipy.org/.

[18] http://wwwasdoc.web.cern.ch/wwwasdoc/minuit/minmain .html.

[19] M. Marchivie, P. Guionneau, J. A. K. Howard, G. Chastanet, J.-F. Létard, A E. Goeta, and D. Chasseau, J. Am. Chem. Soc. **124,** 194 (2002).

[20] V. Briois, Ch. Cartier dit Moulin, Ph. Sainctavit, Ch. Brouder, and A.-M. Flank, J. Am. Chem. Soc. **117,** 1019 (1995).

[21] M. Harmand *et al.*, Nat. Photonics **7,** 215 (2013).

[22] C. Bressler *et al.*, Science **323,** 489 (2009).

[23] N. Huse, H. Cho, K. Hong, L. Jamula, F. M. F. de Groot, T. K. Kim, J. K. McCusker, and R. W. Schoenlein, J. Phys. Chem. Lett. **2,** 880 (2011).

[24] H. T. Lemke *et al.*, J. Phys. Chem. A **117,** 735 (2013).

[25] C. Consani, M. Prémont-Schwarz, A. El Nahhas, C. Bressler, F. van Mourik, A. Cannizzo, and M. Chergui, Angew. Chem., Int. Ed. **121,** 7320 (2009).

[26] W. Gawelda, A. Cannizzo, V.-T. Pham, F. van Mourik, C. Bressler, and M. Chergui, J. Am. Chem. Soc. **129,** 8199 (2007).

[27] M. Chergui in *Spin-Crossover Materials*, edited by M. Halcrow (Wiley, West Sussex, 2013), p. 405.

[28] G. Baranovic and D. Babic, Spectrochem. Acta A **60,** 1013 (2004).

[29] K. L. Ronayne *et al.*, Phys. Chem. Chem. Phys. **8,** 4685 (2006).

[30] M. Buron-Le Cointe, J. Hebert, C. Balde, N. Moisan, L. Toupet, P. Guionneau, J. F. Letard, E. Freysz, H. Cailleau, and E. Collet, Phys. Rev. B **85,** 064114 (2012).

[31] A. Hauser, C. Enachescu, M. L. Daku, A. Vargas, and N. Amstutz, Coord. Chem. Rev. **250,** 1642 (2006).

[32] Y. Kawakami, S. Iwai, T. Fukatsu, M. Miura, N. Yoneyama, T. Sasaki, and N. Kobayashi, Phys. Rev. Lett. **103,** 066403 (2009).

[33] M. Först, C. Manzoni, S. Kaiser, Y. Tomioka, Y. Tokura, R. Merlin, and A. Cavalleri, Nat. Phys. **7,** 854 (2011).

[34] M. Lorenc *et al.*, Phys. Rev. Lett. **103,** 028301 (2009).

[35] M. Lorenc *et al.*, Phys. Rev. B **85,** 054302 (2012).

structure analysis, the pump-probe methods, computations of the density of state and molecular dynamics, and coupled oscillator model. Video S1 shows the breathing mode and video S2 the ligand bending mode of [Fe(phen)$_2$(NCS)$_2$].